



# Constraining asymmetric organometallic catalysts within mesoporous supports ZnPS–BrPPAS boosts their enantioselectivity

Jing Huang <sup>a,c,\*</sup>, Li Yuan <sup>a</sup>, Jiali Cai <sup>b</sup>

<sup>a</sup> Research Center for Advanced Computation, Xihua University, College of Science, Xihua University, Chengdu 610039, PR China

<sup>b</sup> College of Rongchang, Southwest University, Chongqing 402460, PR China

<sup>c</sup> Institute for Clean Energy & Advanced Materials, Southwest University, Chongqing 400715, PR China



## ARTICLE INFO

### Article history:

Received 23 January 2015

Received in revised form 22 June 2015

Accepted 9 October 2015

Available online 22 October 2015

### Keywords:

Chiral Mn(III) salen

Organic–inorganic hybrid material

Unfunctionalized olefins

Heterogeneous catalyst

Asymmetric epoxidation

## ABSTRACT

Novel layered heterogeneous chiral salen Mn(III) catalysts are synthesized with organic–inorganic hybrid material ZnPS–BrPPAS as the support and employed in the asymmetric epoxidations of unfunctionalized olefins. Characterizations indicate that the different linkers could contribute to the morphology varying from schistose structure to spheric particle. The catalysts manifest superior catalytic dispositions (yield, up to >99%; ee, up to >99%) in the epoxidations of olefins such as α-methylstyrene and indene. Moreover, the catalysts could be recovered and reused up to nine times with retention of catalytic dispositions. In addition, the reversal configurations of epoxides are observed with respect to 6-cyano-2,2-dimethylchromene and 6-nitro-2,2-dimethylchromene.

© 2015 Elsevier B.V. All rights reserved.

## 1. Introduction

The transformation of alkenes to corresponding epoxides is both an important industrial technology and a useful synthetic method for a wide range of products including pharmaceuticals and agrochemicals. Chiral Mn(III) salen complexes (Jacobsen's catalyst) have demonstrated very high activity and selectivity for the enantioselective epoxidation of unfunctionalized olefins under homogeneous condition [1–3]. However, such catalysts are not easily recovered for reuse or recycle in homogeneous catalytic systems. Therefore, the heterogenization of chiral Mn(III) salen complexes have received great attention in the last decades due to efficient product purification and easy catalyst recovery [4–15]. Recently, considerable studies have also concentrated on the investigation of inorganic–organic hybrid materials as active heterogeneous catalysts/supports [16,17]. These kinds of materials have the advantage of possessing a broad and non-uniform distribution of pore size, the distribution of functional organic groups or/and catalytic active centers within their framework. Accordingly, the heterogeneous catalysis systems are possessed, not only with high reactivities and enantioselectivities but also easy catalyst/product separation and

simple catalyst recycling. Our research has, for many years, been concerned with metal phosphonate chemistry for catalysts and catalyst supports. Our group have reported the preparation of a series of organic polymer–inorganic hybrid such as ZSPP, ZPS-IPPA, ZPS-PVPA, ZnPS-PVPA and their applications as catalyst supports in immobilizing chiral salen Mn(III) [18–22]. In most cases, these supported chiral Mn(III) salen catalysts indicate comparable or even higher activity and enantioselectivity, compared with the homogeneous counterparts for asymmetric epoxidation. Furthermore, the immobilized catalyst could be reused at least nine times without significant loss of activity.

Mesoporous materials have become attractive materials due to their potential applications as promising materials, such as catalysis, separation, material recognition and hydrogen storage materials. To date, many mesoporous materials have been designed. MCM-41 and SBA-15 are the most frequently used mesoporous materials for the immobilization of homogeneous chiral catalysts. In our group, the layered crystalline ZnPS-PVPA are prepared in mild and facile conditions in water-THF media at 66 °C, entirely apart from the traditional methods. Owing to the layered mesoporous structure, ZnPS-PVPA could be employed as the catalyst supports, enabling one to take advantage of the site isolation effect and the cooperation effect, and bridging the gap between heterogeneous catalysts and homogeneous catalysts [23–28].

However, the effects of organic linkers on the catalytic performance of mesoporous material-supported chiral Mn(III) salen

\* Corresponding author at: Research Center for Advanced Computation, Xihua University, College of Science, Xihua University, Chengdu 610039, PR China.

E-mail addresses: [hj41012@163.com](mailto:hj41012@163.com), [394454290@qq.com](mailto:394454290@qq.com) (J. Huang).

complex have seldom been systematically investigated for the asymmetric epoxidation. Herein, this prompts us to design a novel type of organic–inorganic hybrid material ZnPS–BrPPAS applied in the immobilization of chiral salen Mn(III). The catalytic performance of the supported catalysts, and the effects of the linkers on the morphology and the catalytic activities are systematically discussed in details.

## 2. Experiment

### 2.1. Materials and instruments

(1R,2R)-(-)-1,2-Diaminocyclohexane, 2,4-dihydroxybenzaldehyde, indene,  $\alpha$ -methylstyrene, *n*-nonane, 4-phenylpyridine N oxide (4-PPNO) and sodium hypochlorite were supplied by Alfa Aesar,  $[\text{Br}(\text{CH}_2)_3\text{P}(\text{O})(\text{OEt})_2]$  and  $[\text{Br}(\text{CH}_2)_3\text{P}(\text{O})(\text{OH})_2]$  were prepared according to the procedures by the literature [29], Chiral Jacobsen's catalyst [30], 6-cyano-2,2-dimethylchromene and 6-nitro-2,2-dimethylchromene [31] were synthesized according to the literature procedures.

FT-IR spectra were recorded from KBr pellets using a Bruker RFS100/S spectrophotometer (USA). TG analysis was performed on a SBTQ600 Thermal Analyzer (USA).  $^1\text{H}$  NMR was determined by Bruker AV-300. The interlayer spacings were obtained on DX-1000 automated X-ray power diffractometer, using Cu-K $\alpha$  radiation and internal silicon powder standard with all samples. Scanning electron microscope (SEM) analyses were performed on KYKYEM3200 (KYKY, China) microscopy. The BET surface areas were determined with the use of  $\text{N}_2$  sorption data measured at 77 K (Quantachrome

Autosorb-1). The conversion (with *n*-nonane as internal standard) and the ee values of indene and  $\alpha$ -methylstyrene were measured on GC with Shimadzu GC2014 (Japan) instrument equipped. For the 2,2-dimethylchromenes epoxides, the ee values were determined on HPLC by using a Chiralcel column (OD).

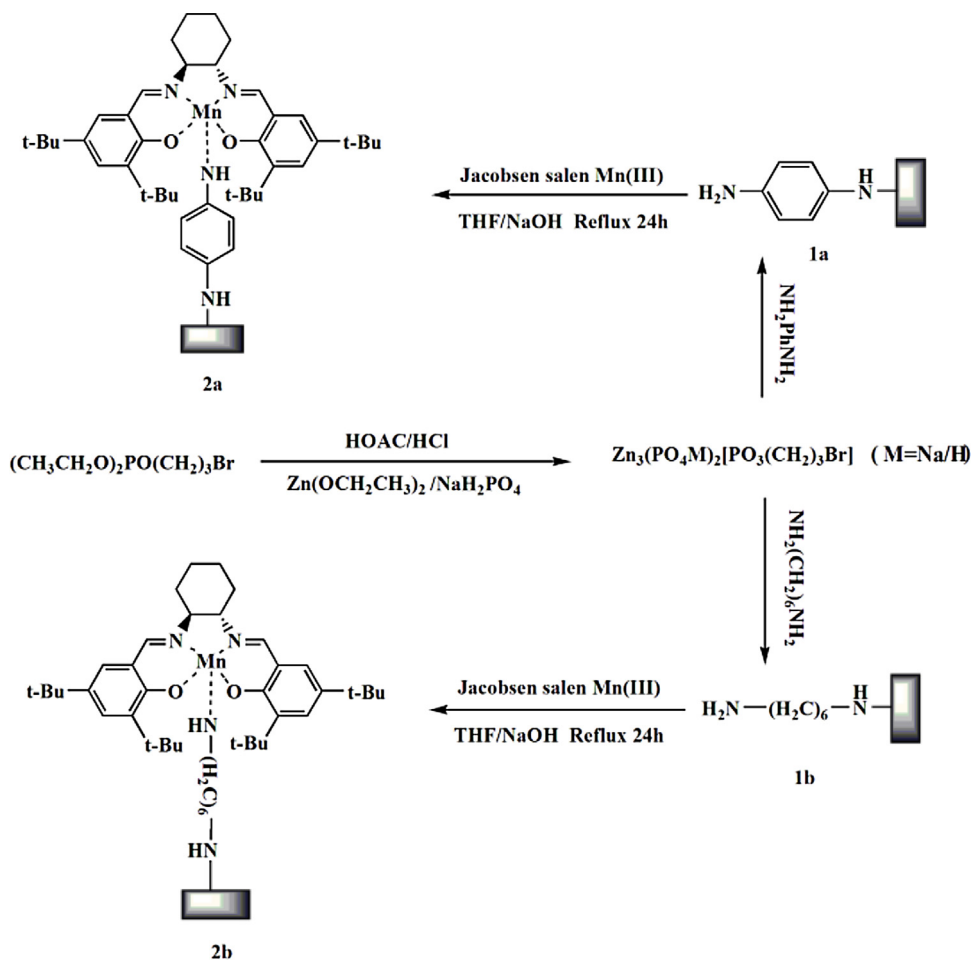
### 2.2. Synthesis of the catalysts (*Scheme 1*)

#### 2.2.1. Preparation of the hybrid zinc 3-bromopropylphosphonatephosphate (ZnPS–BrPPAS)

The mixture of the diethyl 3-bromopropylphosphonate (5 mmol), 8 mL of concentrated hydrochloric acid (36%) and 25 mL of acetic acid was stirred at 80 °C for 24 h, followed by cooling down and evaporating under reduced pressure as well as neutralizing. Sodium dihydrogen phosphate (1.56 g, 10 mmol) in 8 mL of deionized water and zinc acetate (3.29 g, 15 mmol) in 10 mL of deionized water were added while gradually raising the temperature to 66 °C. And then the mixture was retaining for 72 h and laying for another 18 h at room temperature. The white powder zinc phosphonates were obtained by filtering, washing thoroughly with deionized water and drying in vacuum. Yield: 92.0%. Found: C, 5.65; H, 0.92. Calc. for  $\text{C}_3\text{H}_6\text{O}_{11}\text{P}_3\text{BrNa}_2\text{Zn}_3$ : C, 5.70; H, 0.95%.

#### 2.2.2. Synthesis of diamine-modified ZnPS–BrPPAS (1a–b)

The appropriate amount of diamine (such as 1,6-hexamethylenediamine, *p*-phenylenediamine) was mixed with ZnPS–BrPPAS (3.16 g, 0.50 mmol), Et<sub>3</sub>N (0.1 g, 1.0 mmol) and CH<sub>3</sub>CN



**Scheme 1.** Synthetic route for the supported catalysts.

(the molar ratio of diamine to bromine element in ZnPS–BrPPAS is 5:1). After the mixture was kept at 80 °C for 24 h under N<sub>2</sub> atmosphere, the resin-like product was filtered and washed with deionized water. 1a, yield: 76.5%; Found: C, 10.69; H, 1.29; N, 2.77. Calc. for C<sub>9</sub>H<sub>13</sub>O<sub>11</sub>P<sub>3</sub>N<sub>2</sub>Na<sub>2</sub>Zn<sub>3</sub>: C, 16.39; H, 1.97; N, 4.25%. 1b, yield: 72.4%; Found: C, 12.13; H, 2.36; N, 3.15. Calc. for C<sub>9</sub>H<sub>21</sub>O<sub>11</sub>P<sub>3</sub>N<sub>2</sub>Na<sub>2</sub>Zn<sub>3</sub>: C, 16.19; H, 3.15; N, 4.20%.

### 2.2.3. Synthesis of heterogeneous Mn(III) salen catalysts (2a–b)

A solution of chiral salen Mn(III) (2.73 g, 4.30 mmol), 1a (0.50 mmol) and an adequate amount of Et<sub>3</sub>N in THF was vigorously stirred for 24 h under reflux, followed by cooling down and neutralizing as well as evaporating. The product 2a was collected by filtration and washed thoroughly with CH<sub>2</sub>Cl<sub>2</sub> and deionized water as well as dried under vacuum. The sample 2b was gained according to the similar procedure. 2a, yield: 87.6%; Found: C, 36.51; H, 4.33; N, 3.79. Calc. for C<sub>45</sub>H<sub>64</sub>O<sub>13</sub>P<sub>3</sub>N<sub>4</sub>Na<sub>2</sub>Zn<sub>3</sub>Mn: C, 42.96; H, 5.09; N, 4.46%. 2b, yield: 83.5%; Found: C, 33.25; H, 4.43; N, 3.44. Calc. for C<sub>45</sub>H<sub>72</sub>O<sub>13</sub>P<sub>3</sub>N<sub>4</sub>Na<sub>2</sub>Zn<sub>3</sub>Mn: C, 42.69; H, 5.69; N, 4.42%.

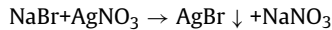
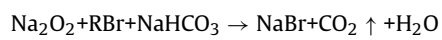
## 3. Results and discussion

### 3.1. Characterizations of the supports and the heterogeneous catalysts

#### 3.1.1. Na and Br content of ZnPS–BrPPAS

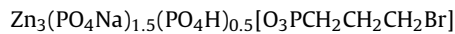
The Na content of the support ZnPS–BrPPAS is 5.5%, which is 0.3% lower than that of theoretical values, could probably be ascribed to pH leading to the ratio of PO<sub>4</sub>Na to PO<sub>4</sub>H.

The chemical equations according to the Br content of are shown below:



R = aliphatic hydrocarbon

The Br content of the support ZnPS–BrPPAS is 12.6%, which is approximate to the theoretical values. On account of this, the empirical formulate of ZnPS–BrPPAS could be denoted as:



#### 3.1.2. Br content of catalysts 2a and 2b

The Br content of the catalysts 2a and 2b is 1.9% and 2.8% respectively. Allowing for the Br content of ZnPS–BrPPAS, it could be deduced that the reactions between ZnPS–BrPPAS and diamine are not complete. Therefore, there are still some residuary Br element in the catalysts 2a and 2b, which are unreacted with diamine.

#### 3.1.3. FT-IR spectra

The FT-IR spectra of the parent support ZnPS–BrPPAS and the heterogeneous catalysts 2a–b are shown in Fig. S1. The strong band at 3400 cm<sup>-1</sup> is ascribed to the –OH, which verifies the presence of surface-bound or intercalated water. The characteristic bands of the chiral Mn(III) salen complexes could be observed in the spectra of heterogeneous catalysts. The bands at 3100, 2300, 1650, 850 cm<sup>-1</sup> are due to C–H vibration of propyl groups and the band assigned to C=N stretching vibrations of chiral Mn(III) salen is seen at around 1630 cm<sup>-1</sup>. The absorption band at 1670 cm<sup>-1</sup> is attributed to N–H plane bending vibration of aromatic amine, which is differentiated to that of the aliphatic amine compound in this region of the spectrum. The strong absorptions at 1400 and 1077 cm<sup>-1</sup> are due to the phosphonate and phosphate stretching vibrations. In addition, after the immobilization of chiral salen Mn(III) onto diamine-modified ZnPS–BrPPAS, the C–Br peak at 550 cm<sup>-1</sup> in the ZnPS–BrPPAS is still could be identified, which confirms the presence of Br element

in the catalysts 2a–b and is in accordance with the results from chemical analysis (AAS).

#### 3.1.4. Powder X-ray diffraction

The powder XRD patterns of the parent support ZnPS–BrPPAS and the heterogeneous catalysts 2a–b (in Fig. 1) display layered crystalline structure. Meanwhile, XRD patterns of ZnPS–BrPPAS manifest a broad 001 peak, accompanied with other peaks at higher-order 00n peaks such as at 35.56°. This also happens to the catalyst 2a–b. Moreover, the part of inorganic phosphate in ZnPS–BrPPAS contributes to the similar patterns at the vicinity of 24.9° to that of Zn<sub>3</sub>(PO<sub>4</sub>)<sub>2</sub>, whose lattice parameters is in accord with the standard data of PDF nos. 29–1390. And the other patterns of ZnPS–BrPPAS such as at 20.8° and 38.2° originate in the section of zinc phosphonate in ZnPS–BrPPAS. Consequently, ZnPS–BrPPAS is not a mixture of zinc phosphonate and zinc inorganic phosphate but hybrid material.

On account of XRD patterns in Fig. 1, the interlayer distances (via the Bragg equation,  $n\lambda = 2d \sin \theta$ ) of ZnPS–BrPPAS and 2a–b are all about 13.3 Å. At the same time, the reflections also display similar peaks, which verifies that the mesoporous structure of the parent support ZnPS–BrPPAS remains intact upon the modification with arylidamine or alkylidamine. In addition, the intensities of diffraction peaks are completely different, which may be ascribed to the different linkers. According to the catalyst 2a, the intensities of diffraction peaks are significantly lower than that of ZnPS–BrPPAS due to the rigid linker p-phenylenediamine; while for the catalyst 2b, the higher intensities of diffraction peaks are owing to the flexible linker 1,6-hexamethylene-diamine. Obviously, the catalyst 2a indicates different crystalline structure to the catalyst 2b. Above all, the special structure of ZnPS–BrPPAS, the isolation effect of linkage as well as the corresponding microenvironment wholly put impacts on the configuration of the catalyst, and may further contribute to the catalytic performance.

#### 3.1.5. Nitrogen adsorption–desorption isotherms

As can be seen in Fig. 2, according to ZnPS–BrPPAS and 2a as well as 2b, the nitrogen adsorption–desorption isotherms are characteristic type V, with a sharp increase in N<sub>2</sub> adsorption at higher  $P/P_0$  values (~0.9) and a distinct hysteresis loop (type H1). And BJH analysis gives a broad and non-uniform distribution of pore size. Some are distributed below 2 nm and some are in the scope of 2–50 nm as well as the others are over 50 nm. On account of the BET treatment of the isotherms, ZnPS–BrPPAS indicates low specific surfaces areas ( $9.2 \text{ m}^2 \text{ g}^{-1}$ ) and pore volume ( $4.3 \times 10^{-2} \text{ cm}^3 \text{ g}^{-1}$ ) as well as

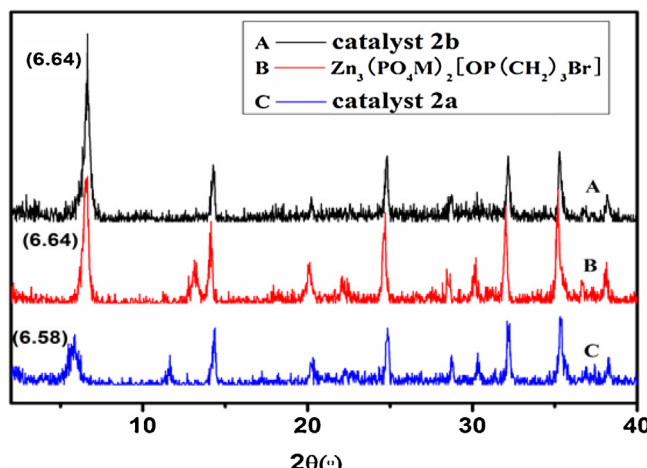


**Fig. 1.** XRD of the heterogeneous catalyst 2b (A), ZnPS–BrPPAS (B) and the heterogeneous catalyst 2a (C).

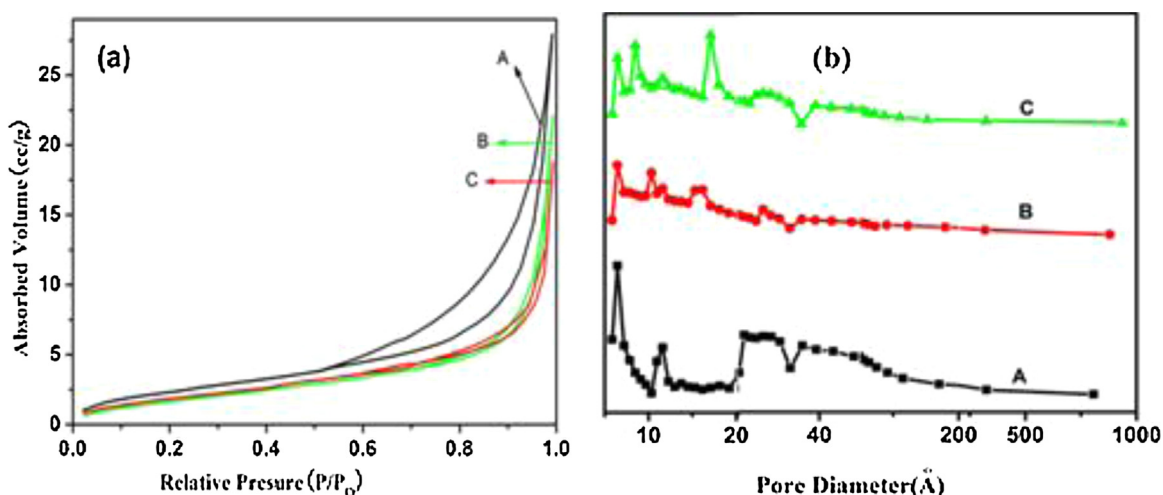


**Fig. 2.** The nitrogen adsorption–desorption isotherm and pore distribution of ZnPS–BrPPAS (A), the heterogeneous catalyst 2b (B) and the heterogeneous catalyst 2a (C).

**Table 1**  
Physicochemical characterization data of ZnPS–BrPPAS, 2a and 2b.

Sample	SBET ( $\text{m}^2 \text{ g}^{-1}$ )	Pore volume ( $\text{cm}^3 \text{ g}^{-1}$ )	Pore size (nm)
ZnPS–BrPPAS	9.2	4.3	9.5
2a	7.6	2.9	7.6
2b	7.0	3.4	8.4

pore diameter (9.5 nm). In view of the size of solvated Mn (salen) Cl complex (2.05–1.61 nm), ZnPS–BrPPAS could provide enough room to accommodate the solvated chiral Mn(III) salen complex. Moreover, the local environment inside the mesopores and the pore size of ZnPS–BrPPAS may throw effects on the enantioselectivity of the epoxidation, which is a crucial property to immobilize active metal complexes such as chiral salen Mn(III).

The corresponding textural parameters calculated by  $\text{N}_2$  adsorption–desorption isotherms are presented in **Table 1**. Upon the amination and the immobilization of chiral salen Mn(III), a remarkable decrease is observed in BET surface area (ZnPS–BrPPAS vs 2a or 2b, from 9.2 to 7.6 or to  $7.0 \text{ m}^2 \text{ g}^{-1}$ ), and in pore volume (ZnPS–BrPPAS vs 2a or 2b, from 4.3 to 2.9 or to  $3.4 \text{ cm}^3 \text{ g}^{-1}$ ) and in pore size (ZnPS–BrPPAS vs 2a or 2b, from 9.5 to 7.6 or to 8.4 nm). On the basis of this, it could be deduced that the steric bulky Mn(III) salen complexes introduced in ZnPS–BrPPAS occupy some caves, holes, nanopores and channels, accompanied with the decrease in these structural parameters.

It is worth noting that different linkers also contribute to the different structure parameters. Pore volume and pore diameter of the catalyst 2a are 10–15% less than that of the catalyst 2b (2a vs 2b: pore volume, 2.9 vs  $3.4 \text{ cm}^3 \text{ g}^{-1}$ ; pore diameter, 7.6 vs 8.4 nm); whereas BET surface area of the catalyst 2a is 10% more than that of the catalyst 2b (2a vs 2b, 7.6 vs  $7.0 \text{ m}^2 \text{ g}^{-1}$ ). According to the configurations of the catalyst 2a–b, the only difference between them is the presence of different diamines linkers. For the catalyst 2b, owing to the flexibility of 1,6-hexamethylenediamine chain, some chiral salen Mn(III) complexes could be immobilized onto the external surfaces of ZnPS–BrPPAS particulates, and other chiral salen Mn(III) complexes might be anchored inside the interlayers or nanopores. In other words, there are two types of the immobilization of chiral salen Mn(III): inner mode and outer mode. With regard to the catalyst 2a, due to the relative rigid linker *p*-phenylenediamine which is difficult to stretch out of the interlayers or mesopores, most of the chiral Mn(III) salen complexes are present inside the nanopores, and seldom are located outside the nanopores. Namely for the catalysts 2a, the chiral salen Mn(III)

complexes are anchored with inner mode. On the whole, the different forms of immobilization of chiral salen Mn(III) are likely to have a significant influence on the asymmetric catalytic performance.

### 3.1.6. Analysis of surface morphology

SEM images of ZnPS–BrPPAS and the heterogeneous catalysts 2a–b are shown in **Fig. 3**. According to ZnPS–BrPPAS, SEM image (**Fig. 3C**) indicates that the diameters of the particles are in the scope of microns. ZnPS–BrPPAS is consisted irregularly of many small and big layered crystalline particles which are aggregates of lots of minor crystalline grains. For the catalyst 2a with rigid *p*-phenylenediamine as the linker, SEM image (**Fig. 3A**) takes on the schistose structure. When the linker changes from rigid to flexible linker 1,6-hexamethylenediamine, SEM image (**Fig. 3B**) for the catalyst 2b accordingly indicates spherical particles with non-uniform size. Similar results have been reported by Choi et al. [32]. In the article, the metal–organic frameworks (MOFs) hybrid metallocopolymers are synthesized by incorporating a homologous series of alkyl side chains to an organic linker such as derivatives of 1,4-benzene dicarboxylic acid with aliphatic side chains at 2,5 positions of the benzene ring, varying from hexyloxy to tetradecyloxy. Moreover, with the increasing of the side chain length, layered polymer tends to form sheets or spheres and further impart a crucial property for processing to the generally intractable metal coordination polymers. Precisely, small changes in the side chain length may lead to large morphological changes. Similarly, different linker could contribute to different morphology and further the ultimate catalytic performance. Spontaneously, a lot of experiments on different types of linkers are needed to conclude this morphology behavior.

### 3.1.7. Mechanism of the formation of catalysts 2a–2b with different morphology

On account of the configuration of ZnPS–BrPPAS, the zinc atoms are located at a plane for every layer, and each zinc atom is bonded to two phosphonate or phosphate along with six oxygen atoms, and every three of these oxygen atoms are bonded to one phosphorus atom. As a result, a minimal unit of the layers of ZnPS–BrPPAS  $\text{Zn}_3(\text{PO}_4\text{M})_2[\text{O}_3\text{PCH}_2\text{CH}_2\text{CH}_2\text{Br}]$  (here M = Na or H) are formed with two phosphonate  $[\text{O}_3\text{PCH}_2\text{CH}_2\text{CH}_2\text{Br}]$  groups denoted as P-G (B) and four phosphate  $(\text{PO}_4\text{M})$  groups designated as P-OM (A) which are bonded to six of zinc atoms. Therefore, ZnPS–BrPPAS is deposited by parallel accumulation of lots of minimal units layer by layer. The ideal model for ZnPS–BrPPAS might be denoted as “AABAABAAB...”. For the catalyst 2a, after the modifica-

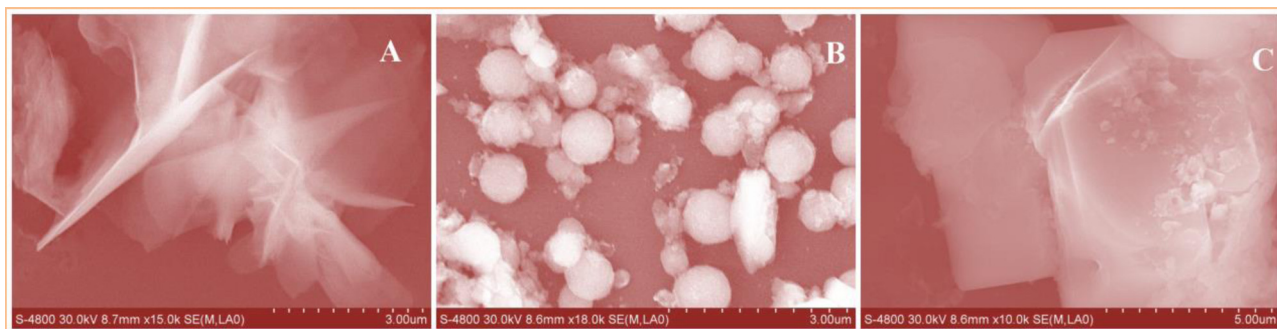


Fig. 3. SEM images of 2a (A), 2b (B) and ZnPS-BrPPAS (C).

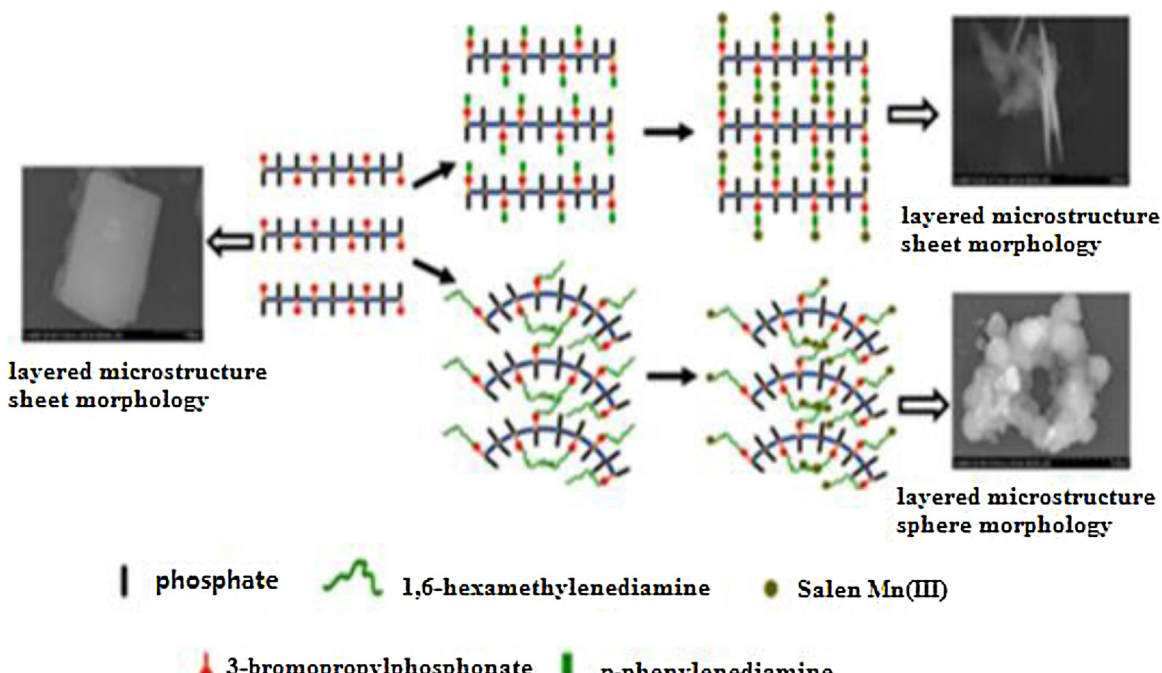


Fig. 4. Analysis of the formation of catalysts with different morphology.

tion of *p*-phenylenediamine linker and the immobilization of chiral salen Mn(III), the relative rigid linkers make the interlayers parallel, which could offer enough space for some substrates approaching the active sites. Meanwhile, the confinement effect generated from steric hindrance among the substrates and active sites is conducive to enhance catalytic performance. While for the catalyst 2b, upon the introduction of 1,6-hexamethylene-diamine linker and chiral salen Mn(III), the parallelity between the interlayers is shattered due to the relative flexible linkers overlapping and twisting, which contributes to the spheroid morphology (Fig. 4).

### 3.2. The asymmetric epoxidation

The heterogeneous catalysts are evaluated in the epoxidations of  $\alpha$ -methylstyrene and indene with NaClO/PPNO as the oxidation system (Table 2). Jacobsen's catalyst is also examined for comparison purposes. The blank experiments indicate that the asymmetric epoxidations hardly occur in the absence of chiral Mn(III) salen complex.

As shown in Table 2, the catalysts 2a–b are active and enantioselective for the epoxidation of  $\alpha$ -methylstyrene (entry 2–3) and indene (entry 7–8). The conversions and ee values are compara-

ble or even higher than those of homogeneous Jacobsen's catalyst (entry 2–3 vs entry 1; entry 7–8 vs 6). According to the asymmetric epoxidation of  $\alpha$ -methylstyrene, the higher ee values than that of the Jacobsen's catalyst (ee%, 97.5– $\geq$  99 vs 65) are achieved by 2a–b (entry 2–3). This may be due to the higher asymmetric induction from the spatial environment between the chiral salen Mn(III) complex and the channels of ZnPS-BrPPAS, which could restrain the free rotation of the intermediate. ZnPS-BrPPAS with a large pore diameter and high periodicity is expected to provide sufficient room to accommodate large chiral salen Mn(III) complexes, which could allow more efficient transport of guest species throughout the three-dimensional catalyst particle. In order to investigate the control of chirality of products, the support ZnPS-BrPPAS and the *p*-phenylenediamine modified ZnPS-BrPPAS 1a are applied to epoxidize  $\alpha$ -methylstyrene under identical conditions. Low olefin enantio excesses are obtained (ee, 0% in entry 4 and 14.6% in entry 5, respectively). On the basis of this, it could be deduced that the support ZnPS-BrPPAS is stereochemically inactive for the epoxidation of olefins and that the linker and chiral salen Mn(III) center contribute to the control of chirality of products. Therefore, the catalytic reactions would not be limited to the catalyst surface only, but be carried out between interlayers and in the nanopores. In

**Table 2**Asymmetric epoxidation of indene and  $\alpha$ -methylstyrene catalyzed by Jacobsen's catalyst and heterogeneous catalysts.<sup>a</sup>

Entry	Catalyst	Substrate <sup>b</sup>	Time (h)	Yield (%) <sup>c</sup>	ee (%)	TOF <sup>e</sup> $\times 10^{-4}$ (s <sup>-1</sup> )
1	Jacobsen's	A	2	>99	65 (S) <sup>d</sup>	27.78
2	2a	A	24	>99	99 (S) <sup>d</sup>	2.31
3	2b	A	24	>99	97.5 (S) <sup>d</sup>	2.31
4	ZnPS-BrPPAS	A	24	>99	0 <sup>d</sup>	2.31
5	1a	A	24	>99	14.6 (S) <sup>d</sup>	2.31
6	Jacobsen's	B	2	98	60 (1S, 2R) <sup>d</sup>	27.22
7	2a	B	24	>99	98.7 (1S, 2R) <sup>d</sup>	2.31
8	2b	B	24	>99	96.6 (1S, 2R) <sup>d</sup>	2.31

<sup>a</sup> Reactions were carried out in CH<sub>2</sub>Cl<sub>2</sub> (1 mL) with alkene (1 mmol), *n*-nonane (internal standard, 1 mmol), PPNO (0.2 mmol), homogeneous (5 mol%) or heterogeneous salen Mn(III) catalysts (5 mol%) and NaOCl (2 mmol).

<sup>b</sup> A =  $\alpha$ -methylstyrene, B = indene.

<sup>c</sup> Conversions were determined by GC, by integration of product peaks against an internal quantitative standard (nonane), correcting for response factors.

<sup>d</sup> Determined by GC with a chiral capillary column (HP19091G-B233, 30 m  $\times$  25 mm  $\times$  0.25 mm).

<sup>e</sup> Turnover frequency (TOF) is calculated by the expression of [product]/[catalyst]  $\times$  time (s<sup>-1</sup>).

**Table 3**Asymmetric epoxidation of 6-cyano-2,2-dimethylchromene and 6-nitro-2,2-dimethylchromene catalyzed by Jacobsen's catalyst and heterogeneous catalysts.<sup>a</sup>

Entry	Catalyst	Substrate <sup>b</sup>	Time (h)	Yield (%)	ee (%) <sup>c</sup>	TOF <sup>d</sup> $\times 10^{-4}$ (s <sup>-1</sup> )
1	Jacobsen's	C	6	60	91 (3R, 4R) <sup>c</sup>	5.56
2	2a	C	24	97	86.7 (3R, 4R) <sup>c</sup>	2.24
3	2b	C	24	51	10.2 (3S, 4S) <sup>c</sup>	1.18
4	Jacobsen's	D	6	68	90 (3R, 4R) <sup>c</sup>	6.30
5	2a	D	24	96	84.3 (3R, 4R) <sup>c</sup>	2.22
6	2b	D	24	45	23.5 (3S, 4S) <sup>c</sup>	1.04

<sup>a</sup> Reactions were carried out in CH<sub>2</sub>Cl<sub>2</sub> (1 mL) with alkene (0.25 mmol), *n*-nonane (internal standard, 1 mmol), PPNO (0.05 mmol), homogeneous (5 mol%) or heterogeneous salen Mn(III) catalysts (5 mol%) and NaOCl (0.5 mmol).

<sup>b</sup> C = 6-cyano-2,2-dimethylchromene, D = 6-nitro-2,2-dimethylchromene.

<sup>c</sup> Chiral HPLC OD column.

<sup>d</sup> Same as in Table 2.

addition, the TOF values for the immobilized catalysts 2a–b are notably lower than those of Jacobsen's (2.31 vs  $27.78 \times 10^{-4}$  s<sup>-1</sup>; entry 2–3 vs 1), which is in accordance with the immobilized catalysts reported in Refs. [33,34]. In most cases, catalytic reactions took a little longer with immobilized catalysts owing to diffusional constraints [35]. On account of the catalytic abilities of ZnPS-BrPPAS and 1a whose conversions both exceeded 99% (entry 4 and 5), it could be deduced that the diffusion is not the rate-limiting step in the whole reaction and the confinement of the support mainly contributes to it.

Apart from the smaller olefin substrates, the heterogenized catalyst 2a–b also indicate superior catalytic activities and enantioselectivities for relatively bulkier olefins, such as indene (ee%, 96.6–98.7 vs 60; entry 7–8 vs 6). This result indicates that the active sites in the channels of immobilized catalyst could be accessed readily by the bulkier reactant.

Table 3 gives the results of the asymmetric epoxidation of 6-cyano-2,2-dimethylchromene and 6-nitro-2,2-dimethylchromene catalyzed by homogeneous Jacobsen's catalyst and heterogeneous catalysts 2a–b. Compared with the results in Table 2, in the epoxidation of 6-cyano-2,2-dimethylchromene, the catalyst 2a also shows ee values comparable to those of the Jacobsen's catalyst, and the catalyst 2b indicates the lower enantioselectivity (2a vs Jacobsen's vs 2b: ee%, 86.7 vs 91 vs 10.2; entry 2 vs 1 vs 3). As for the epoxidation of 6-nitro-2,2-dimethylchromene, the similar results have also been obtained (2a vs Jacobsen's vs 2b: ee%, 84.3 vs 90 vs 23.5). This may be ascribed to the configurations of the catalysts. On account of BET, the catalyst 2a's is larger than that of the catalyst 2b (2a vs 2b, 7.6 vs 7.0 m<sup>2</sup> g<sup>-1</sup>), which could provide enough place to immobilize chiral salen Mn(III) and more chance for the substrates to approach the active sites. While for pore volume and pore size, the catalyst 2a's is smaller than those of the catalyst 2b (pore volume: 2a vs 2b, 2.9 vs 3.4 cm<sup>3</sup> g<sup>-1</sup>; pore size: 2a vs 2b, 7.6 vs 8.4 nm). Additionally, the structure-directing effect from the rigid linker *p*-phenylenediamine and the configurations of the

bulkier substrates contribute to the catalytic performance. When the bulkier substrates such as 6-cyano-2,2-dimethylchromene and 6-nitro-2,2-dimethylchromene approaching the active sites, the confinement effects make the enantioselectivity of the catalyst 2a higher than that of the catalyst 2b [7,36,37].

Notably, the enantioselectivity of the epoxides is significantly reversed upon the asymmetric epoxidation catalyzed by 2a–b. The similar phenomenon has been reported before [38,39]. The catalyst 2a produces 3R, 4R product as the major, which is same to the homogeneous Jacobsen's catalyst; whereas the catalyst 2b gives 3S, 4S product as the dominant. On account of the configurations of 2a and 2b, the difference between them lies in the different linkers. As a matter of fact, the result is not only attributed to the different linkers, but also associated with the confinement effect originated in the nanopores of the catalysts. The whole effect of the support, especially the modes of the immobilization of chiral salen Mn(III) as well as the corresponding microenvironment could restrict the rotation of the intermediates salen Mn(V)=O or transition states of the epoxidation [6,7,25]. Hence, the interaction of the reactants and products could restrict access of reactant to the active site and further influence the stereochemistry of the reaction. In essence, the spatial constraint imposed upon the chiral catalyst by the walls of the pores of the support enhances its asymmetry by predisposing access of the prochiral reactant to the active center and controls the steric configurations of the epoxides. In addition, for the catalyst 2a and Jacobsen's catalyst, the same or similar reaction mechanism detail process contributes to the same configuration of the products; while for the catalyst 2b, the reagents assault or the groups leave in antipodal direction, which form the reversal epoxides. However, the phenomenon does not happen to the asymmetric epoxidations of  $\alpha$ -methylstyrene and indene, where the catalyst 2a–b and Jacobsen's catalyst all give same configurations of epoxides. Namely, the catalysts are selective for the substrates. Certainly, the configuration tumbling due to the different mode of the immobilization remains to be further investigated.

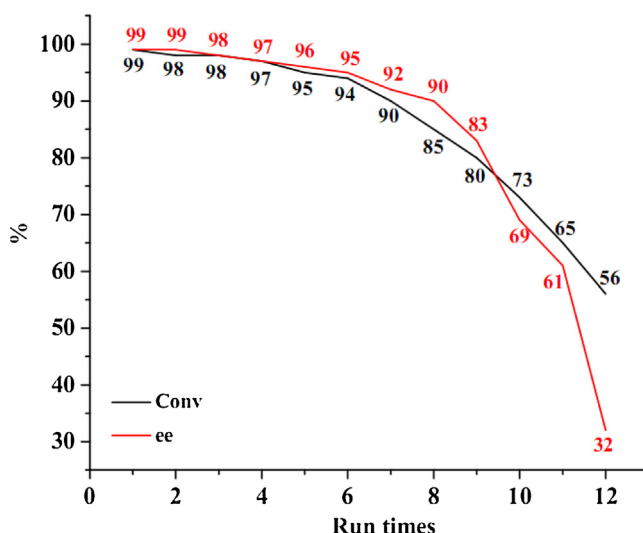


Fig. 5. The recycles of catalyst 2a in the epoxidation of  $\alpha$ -methylstyrene.

### 3.3. The recycling of the supported chiral salen Mn(III) catalyst

To study the stability and reusability of the supported catalyst 2a-b, the recycling experiments are carried out with  $\alpha$ -methylstyrene as a mode substrate (Fig. 5). The catalyst is separated from the reaction mixture after each experiment by simple filtration and washed with water and hexane as well as dried carefully before using it in the subsequent run. Moreover, the filtrates are collected for the determination of Mn leaching. No manganese is detected in the filtrates after the first two runs by AAS. The data in Fig. 5 indicate only a slightly decrease in activity and enantioselectivity after nine consecutive times (conversion: from 99% to 85%; ee: from excess 99% to 90%). In other words, the supported catalyst is provided with superior recyclability, which is comparable to other heterogeneous catalyst under similar condition such as (conversion: 88%; ee: 86.1%; after recycling for nine times) [21–28]. The decrease of the activity could be mainly attributed to several factors, such as the decomposition of the catalysts under epoxidation conditions [40]; the leaching of metal complexes from the materials; the blockage of some pores and channels by organic species from previous runs. The Mn content of the heterogeneous catalyst 2a is 0.36 mmol/g compared with the total amount (around 0.62 mmol/g) when the heterogeneous catalyst recycled for nine times.

## 4. Conclusions

In summary, a novel type of organic–inorganic hybrid material ZnPS–BrPPAS is synthesized and used as catalyst support for immobilizing the chiral salen Mn(III) upon different diamines. Characterizations indicate that the linker could contribute to different morphology, such as schistose structure for the catalyst 2a with rigid *p*-phenylenediamine and spheric particle for the catalyst 2b with flexible 1,6-hexamethylenediamine. The linkers, the support ZnPS–BrPPAS, and chiral salen Mn(III) as well as microenvironment altogether impact catalytic performance. Moreover, the catalysts are selective for the substrates. Apart from this, the catalyst 2a also manifests superior stability and could be recycled for nine times without significant loss of the property, which is provided with the potential applications in industry.

## Acknowledgements

This work is financially supported by the Fundamental Research Funds for the Central Universities (XDK2013C120), the Xihua University Key Projects (Z1223321), Sichuan Province Applied Basic Research Projects (2013JY0090), the Department of Education of Sichuan Province Projects (13ZB0030), Chongqing Special Funding for Postdoctoral (Xm2014028) and Chongqing Postdoctoral Daily Fund (Rc201419).

## Appendix A. Supplementary data

Supplementary data associated with this article can be found, in the online version, at <http://dx.doi.org/10.1016/j.molcata.2015.10.011>.

## References

- [1] W. Zhang, E.N. Jacobsen, *J. Org. Chem.* 56 (1991) 2296.
- [2] K. Noda, R. Irie, Y. Ito, N. Matsusumoto, T. Katsuki, *Tetrahedron Lett.* 31 (1990) 7345.
- [3] K. Srinivasan, P. Michaud, J.K. Kochi, *J. Am. Chem. Soc.* 108 (1986) 2309.
- [4] G.J. Kim, S.H. Kim, *Catal. Lett.* 57 (1999) 139.
- [5] S. Xiang, Y.L. Zhang, Q. Xin, C. Li, *Chem. Commun.* 22 (2002) 2696.
- [6] H.D. Zhang, S. Xiang, C. Li, *Chem. Commun.* 9 (2005) 1209.
- [7] C. Li, H. Zhang, D. Jiang, Q. Yang, *Chem. Commun.* 6 (2007) 547.
- [8] L. Saikia, D. Srinivas, P. Ratnasamy, *Appl. Catal. A* 309 (2006) 144.
- [9] D. Srinivas, P. Ratnasamy, *Microporous Mesoporous Mater.* 105 (2007) 170.
- [10] B.M. Choudary, M.L. Kantam, B. Bharathi, P. Sreekanth, F. Figueras, *J. Mol. Catal. A: Chem.* 159 (2000) 417.
- [11] C. Baleizao, B. Gigante, H. Garcia, A. Corma, *J. Catal.* 215 (2003) 207.
- [12] A.R. Silva, J.L. Figueiredo, C. Freire, B. Castro, *Microporous Mesoporous Mater.* 68 (2004) 83.
- [13] C. Baleizao, B. Gigante, H. Garcia, A. Corma, *Tetrahedron* 60 (2004) 10461.
- [14] B. Gigante, A. Corma, H. Garcia, M.J. Sabater, *Catal. Lett.* 68 (2000) 113.
- [15] B. Bahramian, V. Mirkhani, M. Moghadam, S. Tangestaninejad, *Appl. Catal. A* 301 (2006) 169.
- [16] C. Sanchez, T. Lalot, V. Cabuil, *Chem. Mater.* 13 (2001) 3061.
- [17] Y.F. Yu, S.X. Hou, M. Meng, X.T. Tao, W.X. Liu, Y.L. Lai, B. Zhang, *J. Mater. Chem.* 21 (2011) 10525.
- [18] R.F. Bai, X.K. Fu, H.B. Bao, W.S. Ren, *Catal. Commun.* 9 (2008) 1588.
- [19] K.D. Zou, X.K. Fu, Y.F. Gong, R.Q. Zeng, D. Fu, *J. Funct. Mater.* 38 (2007) 1152.
- [20] X.B. Tu, X.K. Fu, X.Y. Hu, Y.D. Li, *Inorg. Chem. Commun.* 13 (2010) 404.
- [21] B.W. Gong, X.K. Fu, J.X. Chen, Y.D. Li, X.C. Zou, X.B. Tu, L.P. Ma, *J. Catal.* 262 (2009) 9.
- [22] X.C. Zou, X.K. Fu, Y.D. Li, X.B. Tu, S.D. Fu, Y.F. Luo, X.J. Wu, *Adv. Synth. Catal.* 352 (2010) 163.
- [23] J. Huang, X.K. Fu, G. Wang, C. Li, X.Y. Hu, *Dalton Trans.* 40 (2011) 3631.
- [24] W.S. Ren, X.K. Fu, *J. Mol. Catal. A: Chem.* 312 (2009) 40.
- [25] J. Huang, X.K. Fu, Q. Miao, *Appl. Catal. A* 407 (2011) 163.
- [26] J. Huang, X.K. Fu, C.W. Wang, H.Z. Zhang, Q. Miao, *Microporous Mesoporous Mater.* 153 (2012) 294.
- [27] J. Huang, X.K. Fu, Q. Miao, *Catal. Sci. Technol.* 1 (2011) 1472.
- [28] J. Huang, X.K. Fu, G. Wang, Q. Miao, G.M. Wang, *Dalton Trans.* 41 (2012) 10661.
- [29] A.K. Bhattacharya, G. Thyagarajan, *Chem. Rev.* 81 (1981) 415.
- [30] W. Zhang, J.L. Loebach, S.R. Wilson, E.N. Jacobsen, *J. Am. Chem. Soc.* 112 (1990) 2801.
- [31] D. Bell, M.R. Davies, G.R. Geen, I.S. Mann, *Synthesis* 6 (1995) 707.
- [32] E.Y. Choi, C.J. Gao, H.J. Lee, O.P. Kwon, S.H. Lee, *Chem. Commun.* 48 (2009) 7563.
- [33] G.-J. Kim, J.-H. Shin, *Tetrahedron Lett.* 40 (1999) 6827.
- [34] R.I. Kureshy, I. Ahmad, N.H. Khan, S.H.R. Abdi, S. Singh, P.H. Pandia, R.V. Jasra, *J. Catal.* 235 (2005) 28.
- [35] A.R. Silva, K. Wilson, J.H. Clark, C. Freire, *Microporous Mesoporous Mater.* 91 (2006) 128.
- [36] J. Huang, M. Tang, X. Li, G.Z. Zhong, C.M. Li, *Dalton Trans.* 43 (2014) 17500.
- [37] J. Huang, M. Tang, C.M. Li, *RSC Adv.* 4 (2014) 46498.
- [38] R. Raja, J.M. Thomas, M.D. Jones, B.F.G. Johnson, D.E.W. Vaughan, *J. Am. Chem. Soc.* 125 (2003) 14982.
- [39] Y. Wan, P. McMorn, F.E. Hancock, G.J. Hutchings, *Catal. Lett.* 91 (2003) 145.
- [40] C.E. Song, E.J. Roh, B.M. Yu, D.Y. Chi, S.C. Kim, K.J. Lee, *Chem. Commun.* 7 (2000) 615.